Discriminability of tryptophan containing dipeptides using quantum control

Afonina, S.; Nenadl, Ondrej; Rondi, Ariana; Bonacina, Luigi; Extermann, Jérôme; Kiselev, Denis; Dolamic, Igor; Burgi, T.; Wolf, Jean-Pierre

Discriminability of tryptophan containing dipeptides using quantum control

**S. Afonina · O. Nenadl · A. Rondi · L. Bonacina ·
J. Extermann · D. Kiselev · I. Dolamic ·
T. Burgi · J. P. Wolf**

Abstract We show that the coherent manipulation of molecular wavepackets in the excited states of trp-containing dipeptides allows efficient discrimination among them. Optimal dynamic discrimination fails, however, for some dipeptide couples. When considering the limited spectral resources at play (3 nm bandwidth at 266 nm), we discuss the concept of discriminability, which appears uncorrelated to both static spectra and relaxation lifetimes.

1 Introduction

In the quest for label-free bioassays and label-free imaging techniques of biological tissues, coherent control [1, 2] and in particular optimal dynamic discrimination (ODD) [3–5] recently emerged as an attractive novel method. The most relevant biological targets clearly consist of proteins, in which aromatic amino-acids (tryptophan, tyrosine, phenylalanine) provide sensitive fluorescing probes. Tryptophan, for instance, has been widely used for probing protein structures and conformations through its sensitivity to the local nano-environment [6, 7]. Although exhibiting an exceptionally large and dipole sensitive Stokes shift, tryptophan fluorescence could not be efficiently used for discriminating among proteins in an ensemble, because of their strongly overlapping spectra.

ODD demonstrated its capability of discriminating very similar molecules that exhibit almost identical spectra by coherently manipulating the evolution of a molecular wavepacket, excited by an optimally shaped pump laser pulse. However, this demonstration was performed in the visible (on flavins), and the lack of a satisfactory pulse shaping device in the deep UV (DUV, 240–300 nm) limited the access to amino acids and protein absorption. Discrimination was, however, recently achieved among the 2 main fluorescing probes within proteins, tryptophan (trp) and tyrosin (tyr). In this experiment, the two amino acids were in their native unbound form in solution [8]. Using a novel reflective pulse shaping device based on an MEMS (Micro Electro Mechanical System) micromirror array [9, 10], we demonstrate here that discriminating among different trp-containing dipeptides (ala-trp, cyclo(-gly-trp),cyclo(-leu-trp)) is achievable by ODD in the DUV. The task is obviously more demanding than trp/tyr discrimination, since the linear spectra of all considered trp-based dipeptides strongly overlap. We observe that discrimination is more easily obtained for some dipeptide pairs than for others with the limited spectral resources at play (the phase-shaped pump pulse features only 3 nm FWHM at 266 nm). This finding opens the fundamental question of defining novel generic mechanisms of controllability in ODD.

2 Spectroscopic properties of dipeptides

The choice of dipeptides as biomolecular targets for this study has not been only dictated by fundamental motivations, i.e. probing the controllability of the peptide bond of the trp-reporter in protein. Small-peptide-based complexes have also recently emerged as a promising tool for cancer treatment and cancer vaccination [11]. More than 150

S. Afonina · O. Nenadl · A. Rondi · L. Bonacina ·
J. Extermann · D. Kiselev · J. P. Wolf (✉)
GAP-Biophotonics, University of Geneva, 22, ch. de Pinchat,
1211 Geneva 4, Switzerland
e-mail: jean-pierre.wolf@unige.ch

I. Dolamic · T. Burgi
Department of Physical Chemistry, University of Geneva, 30,
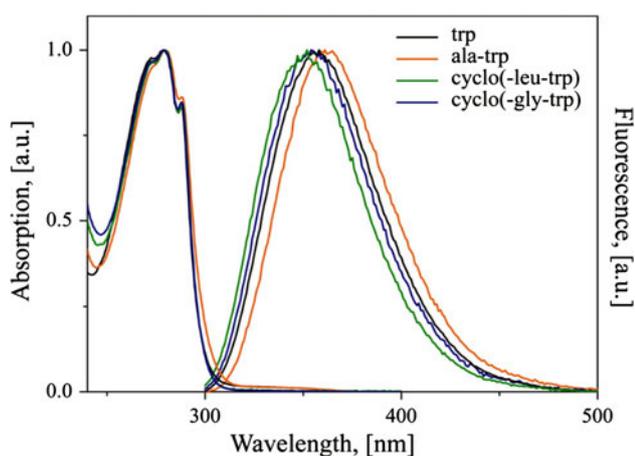quai Ernest-Ansermet, 1211 Geneva 4, Switzerland

Fig. 1 Normalized absorption and fluorescence spectra, measured for the four molecules under consideration at the same molar concentration (1 mM)

patents have been filed to date about these complexes only. Given this prospective use as drugs, the possibility of their label free detection and imaging would be highly appreciated by biologists and biomedical researchers.

As already mentioned, since trp is the optically active element in ala-trp, cyclo(-gly-trp) and cyclo(-leu-trp), their absorption and emission spectra (in water, PH = 7) are dominated by the S_0–>S_1 excitation of the indole ring, and strongly overlap (Fig. 1).

Upon DUV excitation at 266 nm, the largest fluorescence Stokes shift is observed for ala-trp, while cyclo(-gly-trp) and cyclo(-leu-trp) exhibit smaller shifts as compared to free trp in water. Both exposition to water and the link to the second amino acid contribute to these shifts [7].The spectra consist of the weighted contributions from all the conformers associated with each dipeptide [12, 13]. The shifts induced by the peptide bond and the trpnano-environment amount only to some nm and discrimination within a mixture of dipeptides using linear fluorescence is clearly out of reach.

3 Optimal pump-probe fluorescence depletion experiment

To optimally discriminate among these fluorescing dipeptides, we adopted the pump-probe depletion (PPD) approach, which already proved successful for other biomolecules, such as flavins and free amino acids. PPD is based on the time-resolved observation of the competition between excited state absorption (ESA) into higher lying excited states and fluorescence into the ground state. This approach makes use of two physical processes beyond that available in the usual linear fluorescence spectroscopy: (1) the molecular wave packet dynamics in the intermediate

state (S_1) and (2) the transition dipole strength to higher lying excited states (Sn).

More precisely, a first femtosecond pump pulse at 266 nm, coherently excites trp from the ground state S_0 to a set of vibronic levels $S_1\{v'\}$. A molecular wavepacket is formed by coherent superposition of the $S_1\{v'\}$states, the evolution of which is probed by a delayed 800 nm pulse. The second 800-nm femtosecond probe pulse transfers part of the $S_1\{v\}$ population to higher lying electronic states S_n. As S_n states are likely to ionize [14, 15] (autoionization yield: 0.2), the population of S_1 and thus fluorescence to the ground state are irreversibly depleted. To discriminate among different fluorescing molecules using ODD, the DUV pump pulse is optimally shaped so that fluorescence depletion is maximized or minimized for one molecule and not for the others.
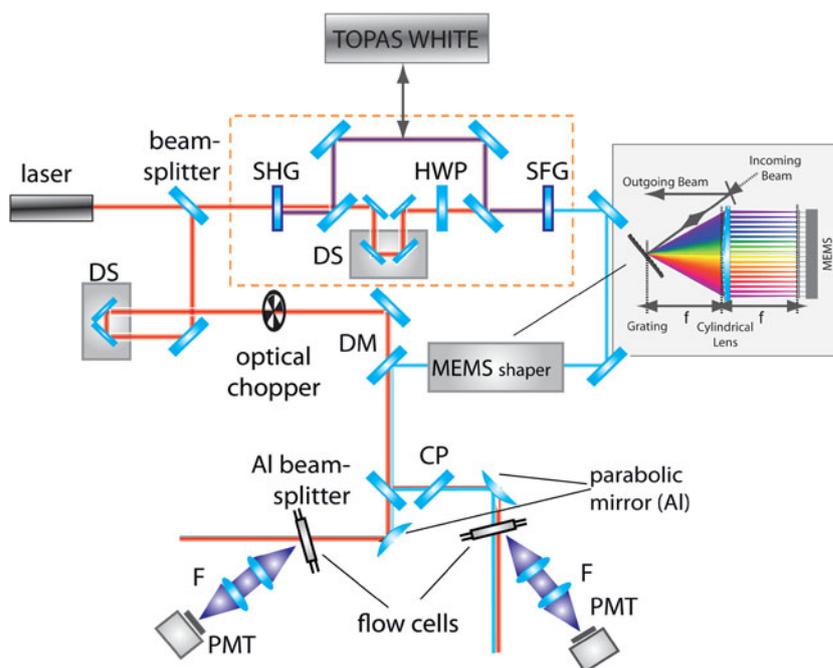
The laser source is a commercial amplified Ti:Sapphire system with a repetition rate of 1 kHz and 27 nm bandwidth centered at 800 nm. As reported in Fig. 2, the beam is split into pump and probe, with the pump frequency passing through a set of doubling and mixing crystals to generate its third harmonic (THG) at 266 nm, which is then sent to the pulse shaper. DUV pulses have a bandwidth of 3 nm FWHM. Shaping is done using a folded 4f shaper, which consists of a highly dispersive grating (3,600 mm^{-1}), an $f = 300$ mm spherical lens, and a MEMS array of 100 Al-coated micromirrors. The MEMS chip, that we specially developed for ODD in the DUV, allows independent stroke and tilt motion of each mirror element for phase and amplitude shaping from the deep UV to the mid IR [7, 16]. With the present arrangement, the spectral resolution at the Fourier plane is 0.1 nm/pixel, allowing a temporal shaping window >2 ps FWHM [17].

The DUV and IR arms are spatially recombined at a dichroic mirror and temporally overlapped by acting on a delay stage placed on the IR path. The experimental cross-correlation is 150 fs. A aluminium coated beam splitter is then used to produce two DUV-IR pulse pairs of equal intensities used to simultaneously interrogate two samples. A compensation plate is inserted in the reflected arm to ensure equal dispersion of the pulses on both arms.

The beams are focused into two identical, home-made, flow-cells, using parabolic Al-coated mirrors, $f = 15$ cm. The flow cells consist of 200-μm thick Sapphire windows and allow for 1 mm light path. Each flow cell contains 1 mM aqueous solutions of the dipeptides (pH 7). Fluorescence is collected using a fused silica lens doublet, $f = 2.5$ cm and $f = 5$ cm, and detected by a photo multiplier placed after a spectrally tailored band-pass filters (350 ± 5 nm). Molecules were obtained as high purity dry powder from Sigma Corporation and Bachem. The powder was dissolved in distilled water.

For pump-wavelength dependence measurements, a frequency-doubled NOPA (Non-collinear Optical Parametric

Amplifier; TOPAS White, Light Conversion inc.) was used in place of the THG stage.

The relative fluorescence variation, $\delta_i(\tau)$, is computed as:

$$\delta_i(\tau) = \left(F_{\text{depl},i}(\tau) - F_{\text{undepl},i}\right)/F_{\text{undepl},i} \qquad (1)$$

where i indicates a specific dipeptide, τ the time delay between UV and IR pulses, F_{undepl} the undepleted fluorescence intensity (i.e. the fluorescence measured in absence of the IR pulse) and $F_{\text{depl}}(\tau)$ the depleted fluorescence (i.e. the fluorescence in presence of the IR pulse). The relative fluorescence variation signal $\delta_i(\tau)$ is calculated on a single-shot basis by averaging typically 1,000 laser shots.

An optical chopper synchronized at half the laser repetition rate placed along the probe path is used for alternating between depleted and undepleted fluorescence measurements. Before each experiment, we ensured that the IR pulse alone was of insufficient intensity to generate fluorescence from direct three-photon absorption. Typical pulse energies at the sample were 0.5 μJ DUV and 5 μJ IR, corresponding to $\sim$20 and $\sim$200 GW cm^{-2} at the focal spot, respectively.

The optimal pulse shape to modify the fluorescence depletion is found using a closed loop approach [18]. The pump-probe time delay τ is adjusted in these optimizations to match the maximum of the time-resolved fluorescence variation, where the dynamics of the molecule can be acted upon the most effectively [6]. The feedback-driven optimization process is based on a multi-objective genetic algorithm described in detail in the previous publications [19, 20].

The resulting optimal pulse shapes were characterized using a down-conversion XFROG (cross frequency resolved optical gating) arrangement. The unshaped 800 nm pulse (110 fs), acting as a reference, was mixed with the 266 nm pulse in a 100-μm thick BBO crystal. The resulting 400 nm was dispersed using a grating (2,400 mm^{-1}) and collimated with a lens ($f = 10$ cm) onto a CCD.

4 Excited state dynamics of trp and trp-containing dipeptides

As previously observed [8], the pump-probe depletion signal from free trp exhibits a very characteristic dip at short time delays peaking at 600 fs (see Fig. 4a and inset of Fig. 3).This feature is absent in the time-resolved fluorescence depletion traces of other biomolecules (tyr [8], riboflavin (RbF), flavin mononucleotide (FMN) [4], adenine [21], etc.). We can then attribute its existence to a specific transient Franck–Condon window opening from the excited S_1 state (^1L_a, ^1L_b) to the S_N manifold (^1B_a, $^1B_2$) [22, 23]. Since the S_N states are strongly auto-ionizing the population of S_1 is depleted and consequently the fluorescence to the ground state. This interpretation was confirmed by selecting a different probe wavelength (400 nm instead of 800 nm),which transfers population to other higher lying excited states than the manifold ^1B_a,$^1B_2$, leads to the disappearance of the dip in the pump-probe transient, which present a step-like behavior in this case.

Given the significance of this time-resolved feature for the discrimination capability of ODD, we further
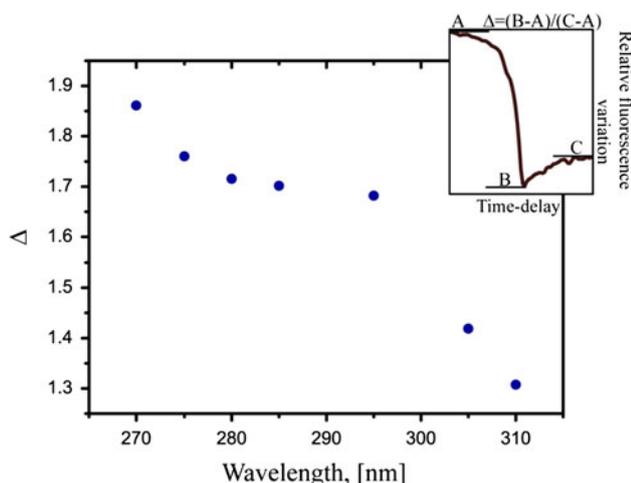
Fig. 3 Related amplitude of the depletion dip feature Δ at short time (B–A) with respect to the long-term depletion level (C–A) as a function of pump pulse wavelength

investigated its spectral behavior upon tuning the pump central wavelength from 270 to 310 nm (using the frequency-doubled NOPA), while keeping the probe fixed at 800 nm.

The results of this procedure are reported in the main plot in Fig. 3. A clear pump wavelength dependence is observed, with a net decrease in the relative amplitude of the depletion dip with respect to the long-term depletion level from 1.87 to 1.3 as the pump pulse wavelength increases from 270 to 310 nm. These measurements therefore confirm the interpretation of a localized Franck–Condon window opening between S_1 and S_n while the intermediate state wavepacket relaxes.

By fitting the time-resolved transients obtained for $\lambda_{pump} = 270$ nm with a function obtained by convoluting a bi-exponential decay with the pump-probe temporal response [24, 25], we find two characteristic exponential decay constants $t_1 = 1.08 \pm 0.050$ ps and $t_2 \gg 500$ ps.

While t_2 relates to the radiative lifetime of the excited state (3.2 ns), t_1 provides information about the short time dynamics within the S_1 hypersurface, and can be ascribed to solvent reorganization. For trp in water, it is well established that relaxation occurs within three timescales [26]: <50 fs, 150 fs and 1 ps. t_1 is in good agreement with the 1 ps timescale, which corresponds to the relaxation of the first solvation shell; namely, to the collective rotational and translational motions of the first layer of water molecules surrounding the solute [27]. The time resolution of our measurements does not allow accessing the two shorter relaxation timescales.

Figure 4 shows how the depletion dynamics is affected by the presence of the second amino-acid in the trp-containing dipeptides (pump: 270 nm, probe: 800 nm). Generally, the dip feature is preserved although the relaxation times t_1 clearly varies due to the additional peptide bond and the modifications of the indole ring nano-environment. Ala-trp and cyclo(-gly-trp) are the least affected among the 3 dipeptides under investigation, yielding the same $t_1 = 1.26 \pm 0.06$ ps, while cyclo(-leu-trp) exhibits a significantly longer time constant $t_1 = 1.71 \pm 0.08$.

The inspection of the depletion traces of Fig. 4 indicate that, although some time constants do vary among the different molecules, time-resolved spectroscopy alone, would not provide sufficient discrimination power for distinguishing between different trp-containing dipeptides or between free trp and dipeptides in a mixture. To increase the discrimination power, we applied coherent control strategies, which already proved successful in the case of flavin molecules [4, 5]. In the riboflavin-FMN case, it was indeed possible to selectively drive a molecular wavepacket onto a location in the adiabatic surface of the ribityl modes, where the IR-probe has a high transition moment towards S_N for FMN and a low one for RbF (and vice versa). A similar situation might arise for dipeptides, since absorption occurs in the indole ring and minute variations associated with the peptide bond can be exploited for ODD.

Fig. 4 Pump-probe fluorescence depletion traces for trp (**a**), ala-trp (**b**), cyclo(-gly-trp) (**c**) and cyclo(-leu-trp) (**d**). The corresponding chemical structures are also shown as *insets*
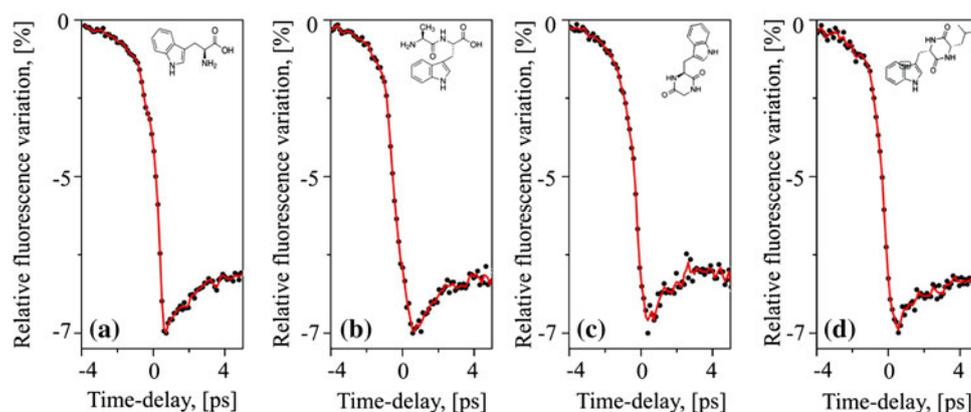
5 Quantum control and optimal coherent discrimination

We first ran a series of feedback driven optimizations aimed at selectivity modifying the depletion amplitude at a given time delay (600 fs) of a defined molecule against another. An exemplary plot summarizing the outcome of an optimization run (ala-trp vs. trp) is shown in Fig. 5. In this case, a multi-objective optimization algorithm was launched with two independent goals: (i) increasing ala-trp-fluorescence and (ii)decreasing trp fluorescence. One can appreciate the result of the procedure by applying the optimal mask on the two samples and acquiring the time-resolved traces, as reported in Fig. 5a and b. In this example, the optimized pulse shape leads to an increase in the ala-trp time-resolved fluorescence variation by 20 %, while trp remains unaffected. Optimization runs with the same objectives were repeated several times to evaluate statistical variations on the results. Note that different pulse shapes were found to lead to similar yields, pointing out the existence of multiple solutions. The closed loop optimization procedure was then performed several times for the opposite set of goals, i.e. (i) decreasing ala-trp-fluorescence and (ii) increasing trp fluorescence. From the comparison of these traces with reference results obtained with Fourier-transform pulses, we establish the histogram presented in Fig. 5c. The coherent manipulation of the molecular wavepacket leads to a variation of discrimination power $DR = \left(\delta_{\text{ala--rp}}^{\text{OPT}} / \delta_{\text{trp}}^{\text{OPT}} \right) / \left(\delta_{\text{ala--trp}}^{\text{REF}} / \delta_{\text{trp}}^{\text{REF}} \right)$ from 0.8 for one pulse shape and 1.08 for the other, tearing apart the trp and ala-trp signatures by more than 8σ (where σ is the averaged

statistical error on the results measured for a defined pulse shape).We also verified that the discrimination power DR was dependent on the time delay τ. As expected for a coherent manipulation of the molecular wavepacket, DR decreases to zero for time delays larger than decoherence time (typically 1.5 ps).

Very valuable information for understanding how the multiobjective optimization process converges is provided by a plot showing the ensemble of solutions after an increasing number of generations. Figure 6 displays such fitness values found by the system after generation 1, 3, 15, 45, 65, and final (converged). The final solutions are represented by the Pareto front highlighted in gray [20]. The
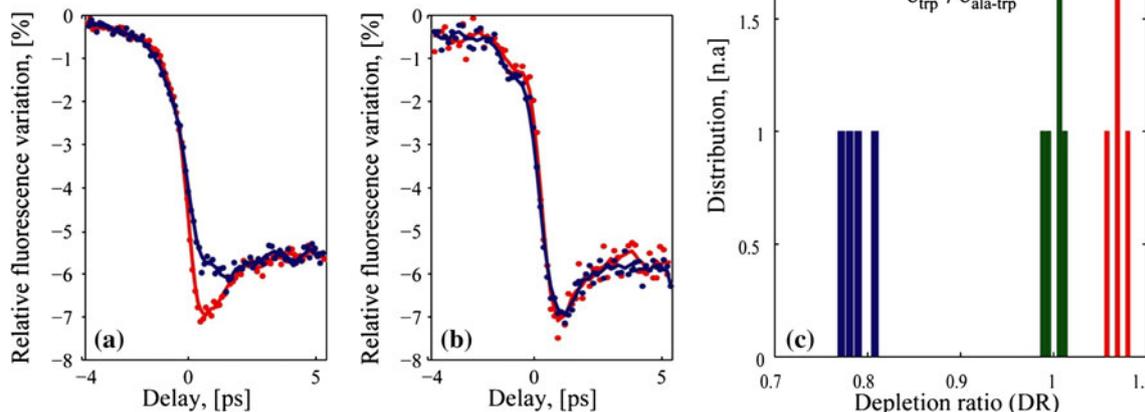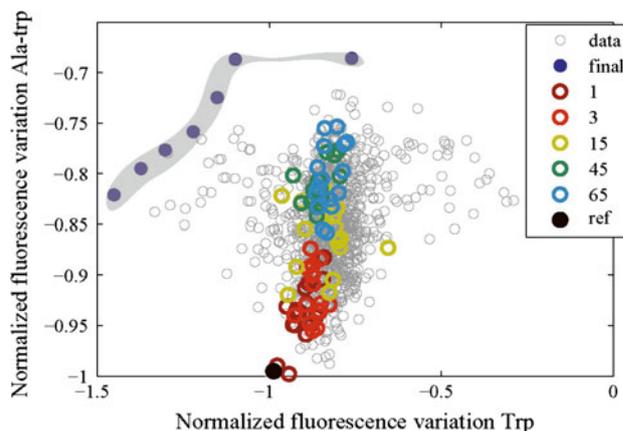

Fig. 6 Pareto front of an optimization for trp against ala-trp. *Blue dots* represent all the solutions sampled during the optimization, *green* highlights the starting first generation of solutions and *magenta* shows the final generation. *Red* shows the non-optimized reference

Fig. 5 Example of successful optimization for fluorescence depletion modulation in case of ala-trp (**a**) versus trp (**b**) with multi-objective algorithm optimization (**c**). Histogram of fluorescence depletions for ala-trp and trp. *Green* (middle column): reference obtained with Fourier-transform pulses, *blue* (*left*): maximization of fluorescence depletion forala-trp, *red* (*right*): maximization of fluorescence depletion for trp

Fig. 7 Histograms of fluorescence depletions for various pairs of molecules. *Green* reference obtained with Fourier-transform pulses, *blue* maximization of fluorescence depletion for row molecule, *red* maximization of fluorescence depletion for column molecule
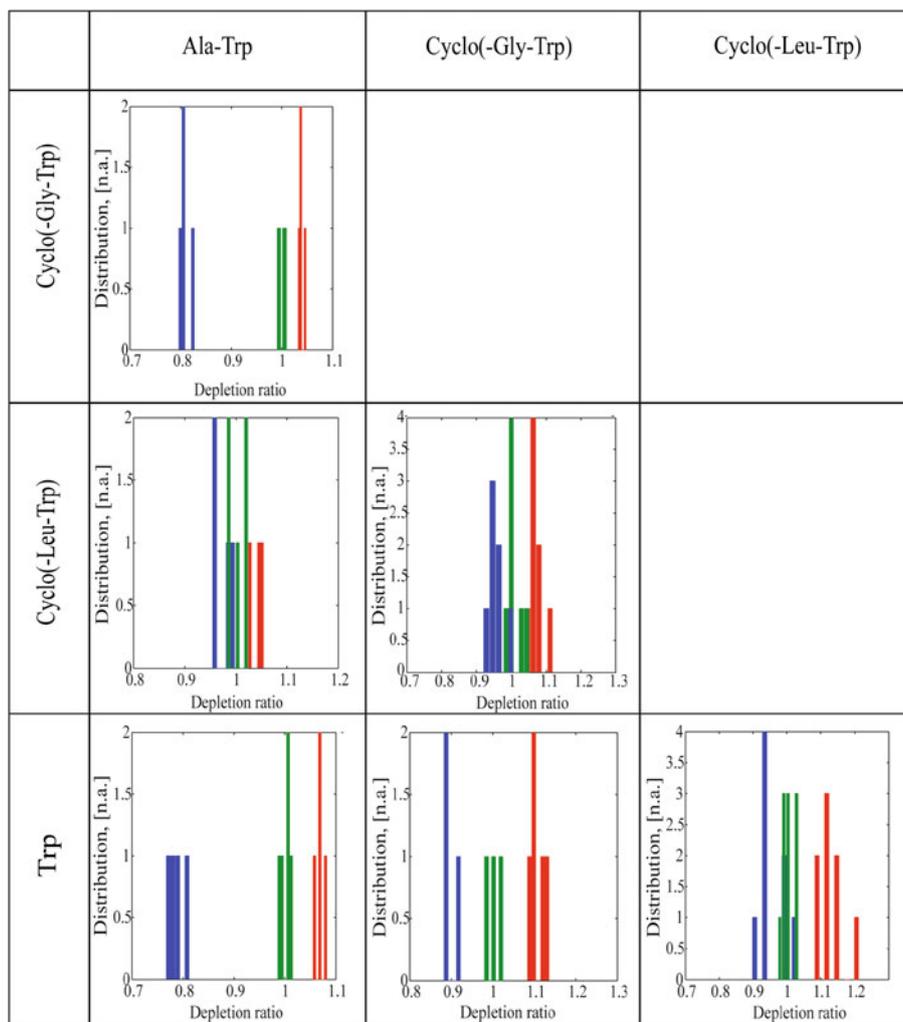
presence of multiple solutions instead of a single one indicates that for this problem it is impossible to find a unique pulse shape which simultaneously performs optimally for both targets [19]. Disposing of an ensemble of solutions in the Pareto front allows, however, for choosing between a pulse shape that maximizes the fluorescence of ala-trp or minimizes the fluorescence of trp (in this specific case).

The same procedure described above was applied to all pairs of dipeptides and free trp, giving rise to the matrix displayed in Fig. 7:

In the histograms, bars indicate the ratios of the depletion values (row molecules over column molecules) obtained using phase-shaped DUV pulses retrieved by optimizations aimed at minimizing (blue) or maximizing (red) this quantity. Green bars correspond to the ratio of the depletion values measured with unshaped pulses. One can see that for several molecule pairs (trp vs. dipeptides, cyclo(-gly-trp) vs. ala-trp) the discrimination capability of the method is satisfactory, with a fluorescence difference

between the optimized pulse shapes ranging from 3σ (trp vs. cyclo(-leu-trp)) to 8σ (cyclo(-gly-trp) vs. ala-trp), which is remarkably high considering the modest bandwidth available for the shaped DUV pulse. This restricted parameter space does not allow, in opposite, to discriminate other dipeptides like cyclo(-leu-trp) vs. ala-trp.

To further test the specificity and robustness of the discrimination experiments, we evaluated the discrimination capability of our method on a mixture of peptides in solution (Fig. 8). First, we applied the reference, unshaped pulse, on cyclo(-gly-trp) (A), cyclo(-leu-trp) (B), and to a 1:1 mixture of cyclo(-gly-trp) and trp (C). We then calculated the Δ factor introduced in Fig. 3. The latter is very similar for the three samples (about 1.2), in perfect agreement with the traces of Fig. 4, which were established in similar conditions. We then applied a pulse shape obtained by optimizing the following targets: decreasing cyclo(-leu-trp) fluorescence and increasing cyclo(-gly-trp) fluorescence. As observed in other optimization runs, the application of this phase mask on cyclo(-leu-trp) yields a
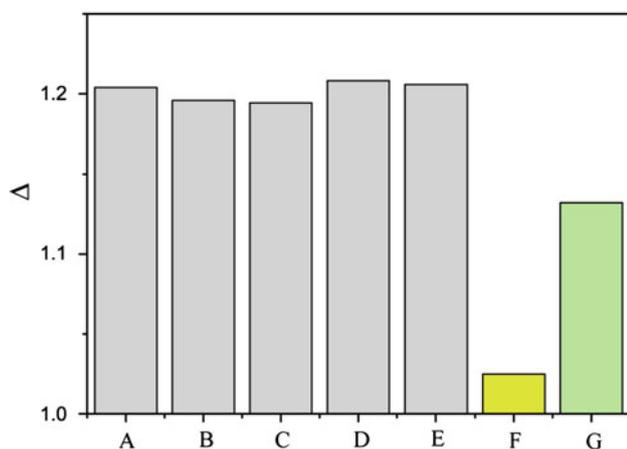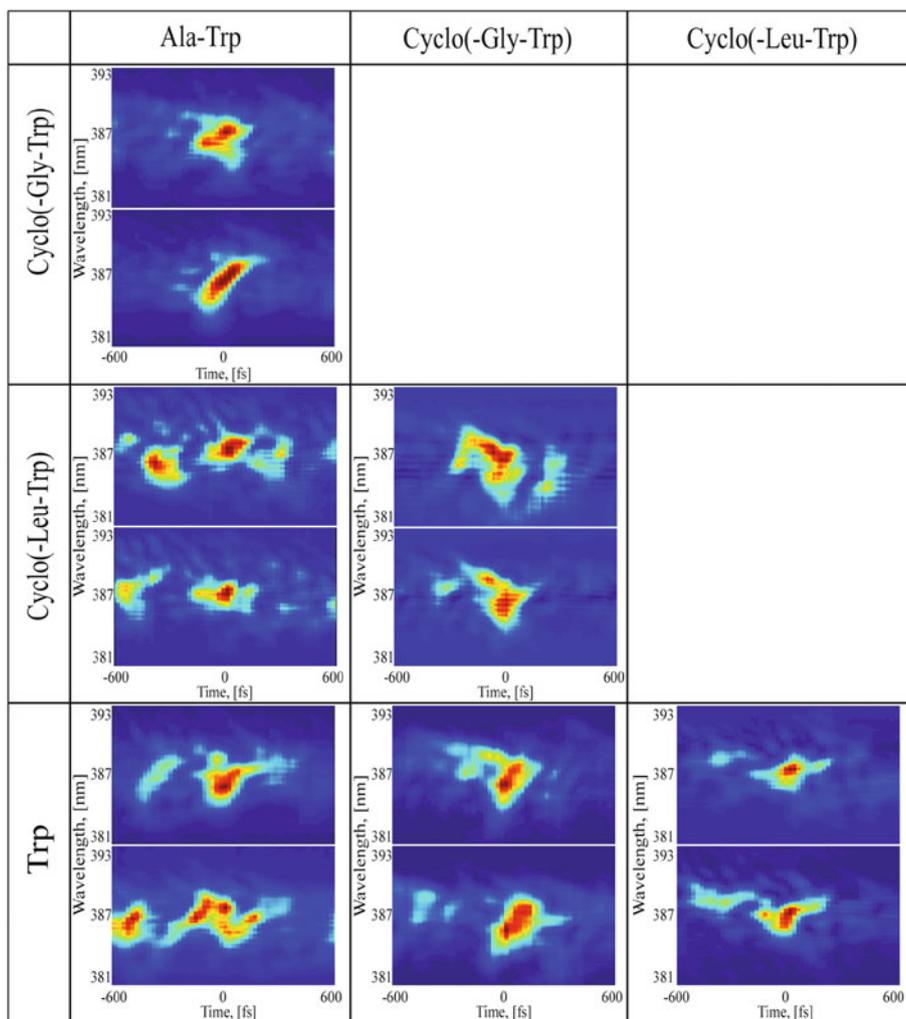
Fig. 8 Resulting depletion signal of cyclo(-gly-trp) and trp mixture with optimized mask for increasing cyclo(-gly-trp) fluorescence and decreasing cyclo(-leu-trp) fluorescence. **a** cyclo(-gly-trp) with unshaped pulse, **b** cyclo(-leu-trp) with unshaped pulse, **c** 1:1 cyclo (-gly-trp)/trp mixture with unshaped pulse, **d** cyclo(-leu-trp) with optimized mask, **e** trp with mask for cyclo(-gly-trp) and cyclo (-leu-trp), **f** cyclo(-gly-trp) with optimized mask, **g** 1:1 cyclo(-gly-trp)/trp mixture with mask for cyclo(-gly-trp) and cyclo(-leu-trp)

relatively poor effect with a very modest increase in the Δ factor (a few percents) for this dipeptide, similar, for example, to the effect shown in Fig. 5b. Likewise, the application of this mask to trp does not yield any significant variation in the time-resolved fluorescence response of the aminoacid. Conversely, when applying the same pulse shape to cyclo(-gly-trp), we observe a significant decrease in the Δ factor of the dipeptide (down to 1.3, i.e. an almost disappearance of the depletion dip) consistent with the second optimization target and pointing to the high specificity of the retrieved phase-mask. The same mask has also been applied to the 1:1 trp/cyclo(-gly-trp) mixture yielding a Δ factor lying in between the results obtained for the separated molecules. This finding supports the possibility to use a sequence of masks optimized for different molecules for determining their relative concentrations in a mixture [4].

In most cases, the optimal pulse shapes measured by X-FROG (Fig. 9), consist of complex multi-structures, but in some specific situations (cyclo(-gly-trp) vs. ala-trp) a single chirped pulse seems to be sufficient for

Fig. 9 XFROGs of pulse shapes that lead to optimal discrimination. In each box, the image on the *top* is for maximising the fluorescence signal for the molecule in a respective row with the molecule in the respective column being minimised, and vice versa for the image below (same ordering as in Fig. 7)

discrimination. By considering the pulse sequences observed in some cases, characteristic frequencies could be retrieved, which might serve for impulsive driving of the molecular wavepacket in S_1 (see next section). Although it is tempting to think that each optimal pulse shape could correspond to a specific conformer of the dipeptides, we found the same diversity of solutions for the flavin case previously. The solution manifold only expresses that different paths are able to yield the same discrimination power. Theoretical calculations similar to those performed for the flavins experiment [5] are certainly necessary for understanding the underlying interaction mechanisms leading to the coherent discrimination of selected pairs of peptides. On the other hand, it would be highly desirable to assess some general criteria allowing one to predict the ODD-discriminability of an ensemble of molecules.

6 The track towards molecular discriminability criteria

It is clear from Fig. 7 that even for a group of very similar molecules addressed with identical experimental resources (laser spectral bandwidth as compared to absorption bandwidth, shaping spectral resolution), large variations do occur. No obvious reason emerged from our measurements. For instance, no correlation exists between the Stokes shifts in the static spectra and discriminability: although trp and cyclo(-gly-trp) exhibit the closest absorption/fluorescence spectra, discrimination was easily achieved, in contrast to cyclo(-leu-trp) and ala-trp for which ODD proved unsuccessful even after several optimization runs, although they present the least overlapping spectra of the series. Similarly, purely dynamical considerations, based on the time-resolved measurements summarized in Fig. 4, would suggest that, for instance, ala-trp should be more easily distinguished from cyclo(-leu-trp) (different relaxation time constants) than from free trp, which is not the case.

As our coherent control experiment relies on coherence between several vibronic states, we investigated whether discriminability could be assessed via correlations and anti-correlations between vibrational spectra of the different peptides. In this respect, THz and far IR absorption spectra of the molecules have been measured using a Bruker FTIR spectrometer (Fig. 10). It has to be noticed, however, that these spectra are representative of the low frequency vibrational modes of the ground states and that they were acquired for molecules in dry form (because of the strong water absorption in the 10–500 cm^{-1} region).

Although the frequency range addressable by the bandwidth of our DUV laser (0–450 cm^{-1}) is rather limited, clear differences are observed between the 4 vibrational spectra. No assignment of the bands is available from the literature, although modes have been identified for
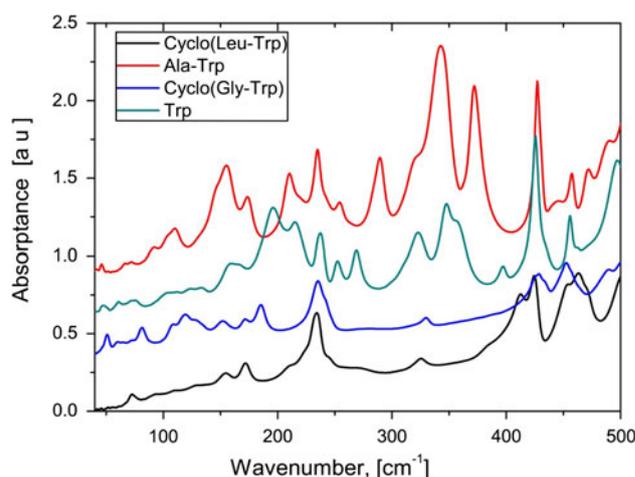

Fig. 10 Far-infrared absorption spectra of (from *top* to *bottom*): ala-trp, trp, cyclo(-gly-trp) and cyclo(-leu-trp)

free amino acids [28], especially trp. In trp (also in dry form), strong bands are observed at 196 and 347 cm^{-1}, associated with hydrogen bond modes and CC$^{\alpha}$N deformations, respectively, while numerous lower frequency and weaker modes reflect further hydrogen bond modes and torsion of the entire side chain about the C-ring bond.

From a qualitative analysis of the correlations between the spectra, the following conclusions can be drawn: (1) trp is clearly discriminable from all dipeptides; (2) ala-trp also exhibits a highly structured spectrum, which is discriminable from all others too; cyclo(-leu-trp) and cyclo(-gly-trp) are the most difficult molecules to distinguish, although some differences are apparent in the very low frequency range (10–150 cm^{-1}).The vibrational discriminability, therefore, agrees to some extent to the discrimination power found in the quantum control experiment displayed in Fig. 7 (except for the ala-trp vs. cyclo(-leu-trp)). However, the comparison cannot be extended further, since characteristic frequencies extracted from the corresponding pulse trains of Fig. 9 (e.g., depending on the molecule pair to be distinguished, 50 ± 5 cm^{-1}, 65 ± 5 cm^{-1}, 105 ± 5 cm^{-1}, 200 ± 5 cm^{-1}, 350 ± 5 cm^{-1}) are found to match some specific vibrational transitions of the, respectively, involved molecules only in some cases, but not systematically. This is not surprising since the measured FIR-spectra address frequencies in the ground state and not in the excited state. Moreover, the spectra are certainly affected by the different environments (dry powder vs. solution). Finally, the complexity of the needed manipulation of the molecular wavepacket widely exceeds impulsive excitation schemes. The pulse shape needs, indeed, to drive the wavepacket at some specific location of the S_1 hypersurface in a time corresponding to the arrival of the probe pulse, where the dipole moment to S_n is comparatively more favorable for one molecule than for the other.

To avoid confusion, let us finally notice that the strength of our fluorescence-based approach is its extreme sensitivity (ultimately down to the single molecule level [29]) and its applicability to peptides/proteins in water, whereas discrimination using far infrared spectroscopy would be limited to larger amounts of proteins in dry form.

7 Conclusions

In conclusion, we have applied the ODD approach to perform phase-sensitive fluorescence-based identification of aqueous solutions of trp-containing dipeptides which present strongly overlapping absorption and fluorescence spectra. We ran a series of discrimination optimizations on six pairs of samples. In four cases, the optimizations were successful, and the resulting pulse shape was able to exert a clear difference in the time-resolved fluorescence response well above the experimental noise and the measurement reproducibility. In two other cases, we were not able to distinguish the molecules. Although comparison with low-frequency vibrational spectroscopy provides useful complementary information, no direct correlation was found between discrimination capability and static spectral properties and dynamic relaxation times. These considerations stress out that coherence is the key parameter in ODD, and that neither static spectroscopy nor purely dynamical investigations are straight fully linked to optimal discrimination.

References

1. C.H. Tseng, T.C. Weinacht, A.E. Rhoades, M. Murray, B.J. Pearson, Opt. Express **19**, 24638 (2011)
2. A.C.W. van Rhijn, A. Jafarpour, M. Jurna, H.L. Offerhaus, J.L. Herek, Faraday Discuss. **153**, 227 (2011)
3. B.Q. Li, G. Turinici, V. Ramakrishna, H. Rabitz, J. Phys. Chem. B **106**, 8125 (2002)
4. M. Roth, L. Guyon, J. Roslund, V. Boutou, F. Courvoisier, J.P. Wolf, H. Rabitz, Phys. Rev. Lett. **102**, 253001 (2009)
5. J. Petersen, R. Mitric, V. Bonacic-Koutecky, J.P. Wolf, J. Roslund, H. Rabitz, Phys. Rev. Lett. **105**, 073003 (2010)
6. S. Schenkl, F. van Mourik, G. van der Zwan, S. Haacke, M. Chergui, Science **309**, 917 (2005)
7. J.T. Vivian, P.R. Callis, Biophys. J. **80**, 2093 (2001)
8. A. Rondi, L. Bonacina, A. Trisorio, C. Hauri, J.P. Wolf, Phys. Chem. Chem. Phys. **14**, 9317 (2012)
9. S.M. Weber et al., Rev. Sci. Instrum. **82**, 075106 (2011)
10. S.M. Weber, J. Extermann, L. Bonacina, W. Noell, D. Kiselev, S. Waldis, N.F. de Rooij, J.P. Wolf, Opt. Lett. **35**, 3102 (2010)
11. O. Mandelboim, E. Vadai, M. Fridkin, A. Katzhillel, M. Feldman, G. Berke, L. Eisenbach, Nat. Med. **1**, 1179 (1995)
12. A.S. Eisenberg, L.J. Juszczak, J. Amino Acids **2012**, 735076 (2012)
13. I. Hunig, K. Kleinermanns, Phys. Chem. Chem. Phys. **6**, 2650 (2004)
14. H.B. Steen, J Chem. Phys. **61**, 3997 (1974)
15. H. Lippert, V. Stert, L. Hesse, C.P. Schulz, I.V. Hertel, W. Radloff, Chem. Phys. Lett. **376**, 40 (2003)
16. J. Extermann, S.M. Weber, D. Kiselev, L. Bonacina, S. Lani, F. Jutzi, W. Noell, N.F. de Rooij, J.P. Wolf, Opt. Express **19**, 7580 (2011)
17. A.M. Weiner, Rev. Sci. Instrum. **71**, 1929 (2000)
18. R.S. Judson, H. Rabitz, Phys. Rev. Lett. **68**, 1500 (1992)
19. L. Bonacina, J. Extermann, A. Rondi, V. Boutou, J.P. Wolf, Phys. Rev. A **76**, 023408 (2007)
20. K. Deb, A. Pratap, S. Agarwal, T. Meyarivan, IEEE T Evolut. Comput. **6**, 182 (2002)
21. A. Rondi (2012) PhD thesis of the University of Geneva
22. D.M. Rogers, J.D. Hirst, J. Phys. Chem. A **107**, 11191 (2003)
23. A. Roy, P. Bour, T.A. Keiderling, Chirality **21**, E163 (2009)
24. I.H.M. van Stokkum, D.S. Larsen, R. van Grondelle, BBA Bioenergetics **1658**, 262 (2004)
25. I.H.M. van Stokkum, D.S. Larsen, R. van Grondelle, BBA-Bioenergetics **1657**, 82 (2004)
26. R. Jimenez, G.R. Fleming, P.V. Kumar, M. Maroncelli, Nature **369**, 471 (1994)
27. M. Maroncelli, J. Macinnis, G.R. Fleming, Science **243**, 1674 (1989)
28. A. Matei, N. Drichko, B. Gompf, M. Dressel, Chem. Phys. **316**, 61 (2005)
29. R. Hildner, D. Brinks, N.F. van Hulst, Nat. Phys. **7**, 172 (2011)